Use of SANS to study hard-matter (non-polymer, non-biological systems

Ken Littrell

GP SANS Instrument Scientist

HFIR/NSSD Oak Ridge National Laboratory

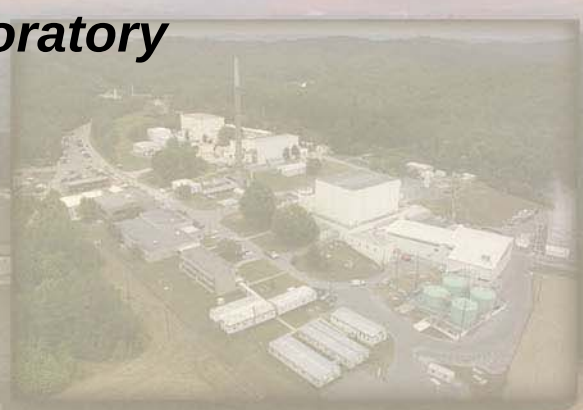

OAK RIDGE NATIONAL LABORATORY
U. S. DEPARTMENT OF ENERGY

Systems that will be discussed today

- **Nanophase catalytic materials**
- **Catalytic and adsorbent carbons**
- **Glasses**
- **Geophysical samples**
- **Structural/industrial alloys**
- **Nanoscale magnetic effects in bulk materials**
- **Superconductivity**

All of these systems contain structure and ordering with length scales ranging from Å to μm or larger

Nanophase catalytic materials: Zirconia

- **high melting point (about 2700°C)**
- **high corrosion resistance**
- **high ionic conductivity**
- **rich in acidic and basic active sites**

Work done at Argonne with Li Xiaohe (UK) and students, CK Loong Thiyaga (IPNS)

What Is Small Angle Scattering?

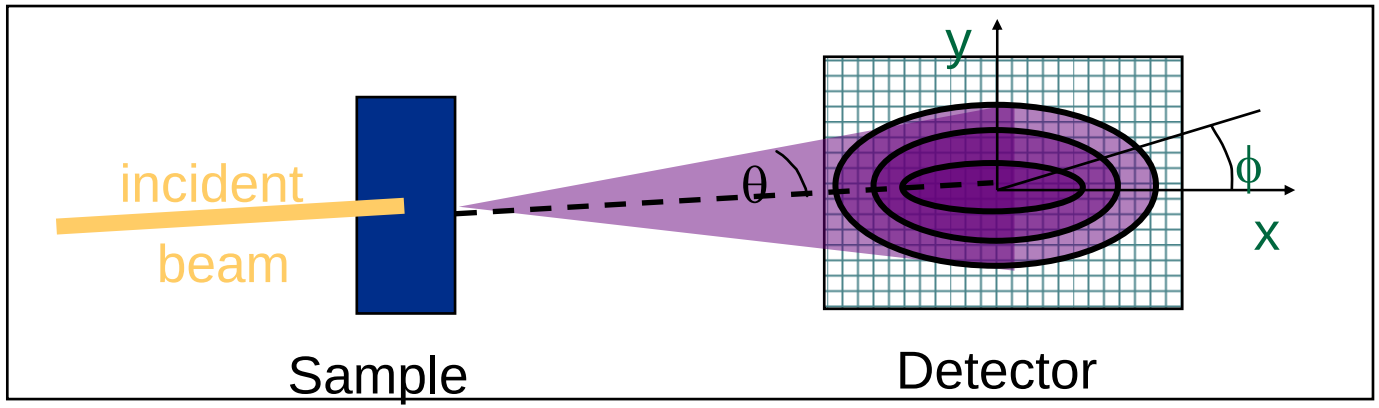

$$I(Q) = A\,\Delta\rho^2\,n\,V^2\,P(Q)\,S(Q)$$

Calibration

Isotope labeling (6.34E10 cm^{-2} for D_2O and -0.56E10 cm^{-2} for H_2O)

$$R = \frac{2\pi}{Q} \quad ; \quad Q = \frac{4\pi}{\lambda}\cdot\sin\frac{\theta}{2}$$

λ is neutron or x-ray wavelength

Probes length scales of ~ 0.5 - 100 nm

Using angles of θ = 0.5 to 5°

A powerful tool for studying disordered bulk materials (solid and solution phases)

Information from SAS

- **Size**
- **Shape**
- **Molecular Weight**
- **Interaction distances**
- **Self Assembly**
  - **Phase transition**
  - **Thermodynamics**
  - **Reaction kinetics**
- **Crystallization**
- **Fractal Dimension**

Reverse micelle method provides a favorable microenvironment for controlling the chemical reaction

Amphiphilic Surfactants

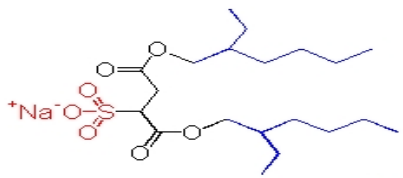

Aerosol OT

Amphiphilic surfactants contain a non-polar portion and a polar portion.

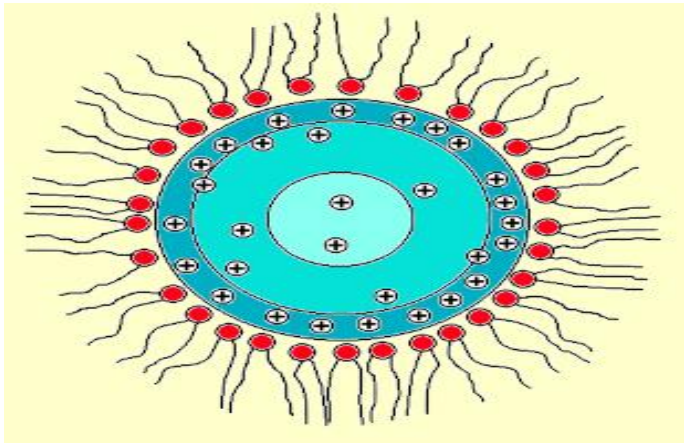

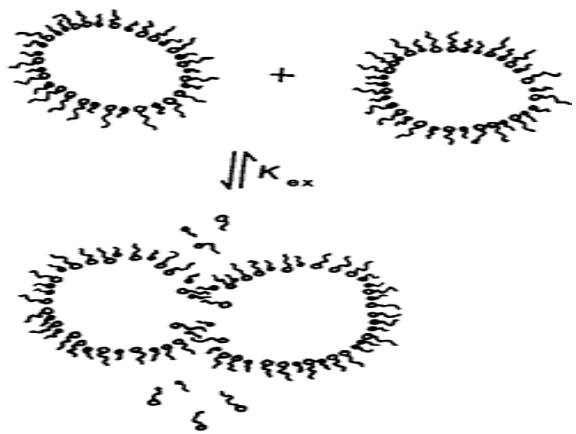

TEM studies of nanophase zirconia prepared using the reverse micelle synthesis method

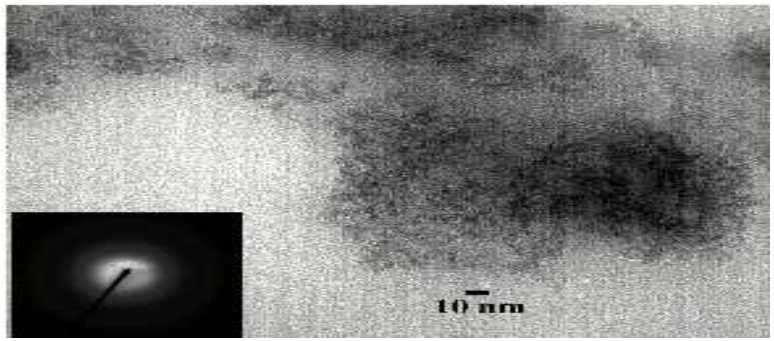

Gel

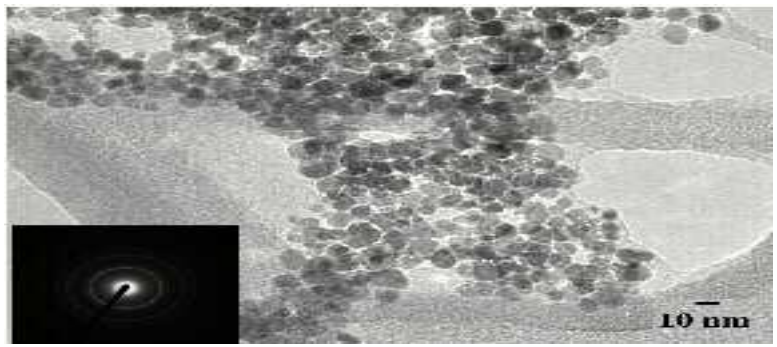

After calcination

Reverse micelle method

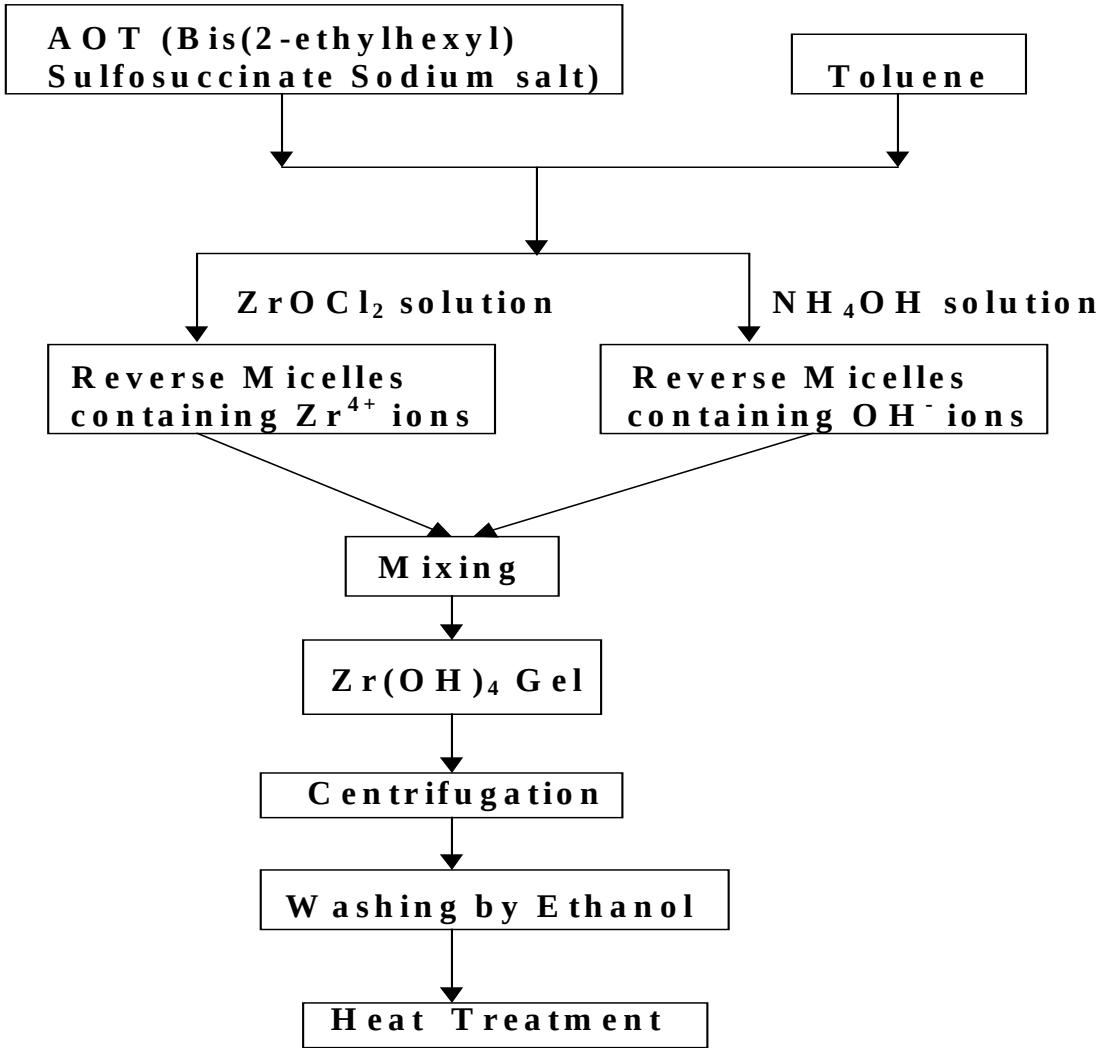

Sol-gel method

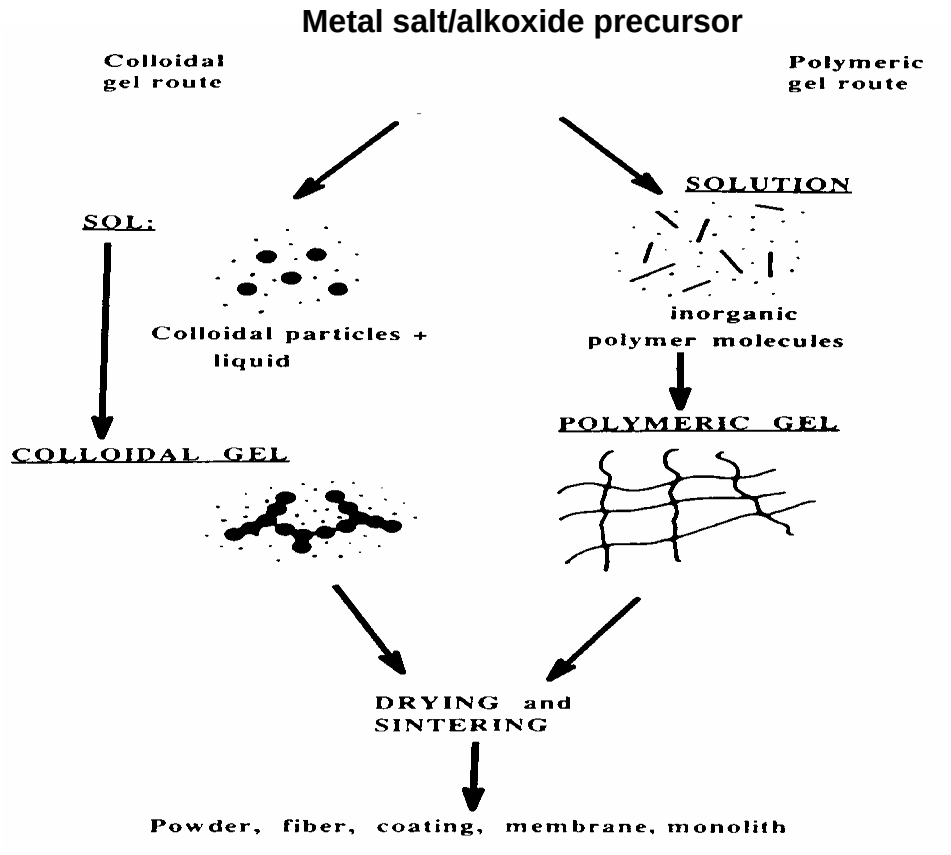

Effects of heat treatment on zirconia powders produced using the sol-gel (hydrolysis) method

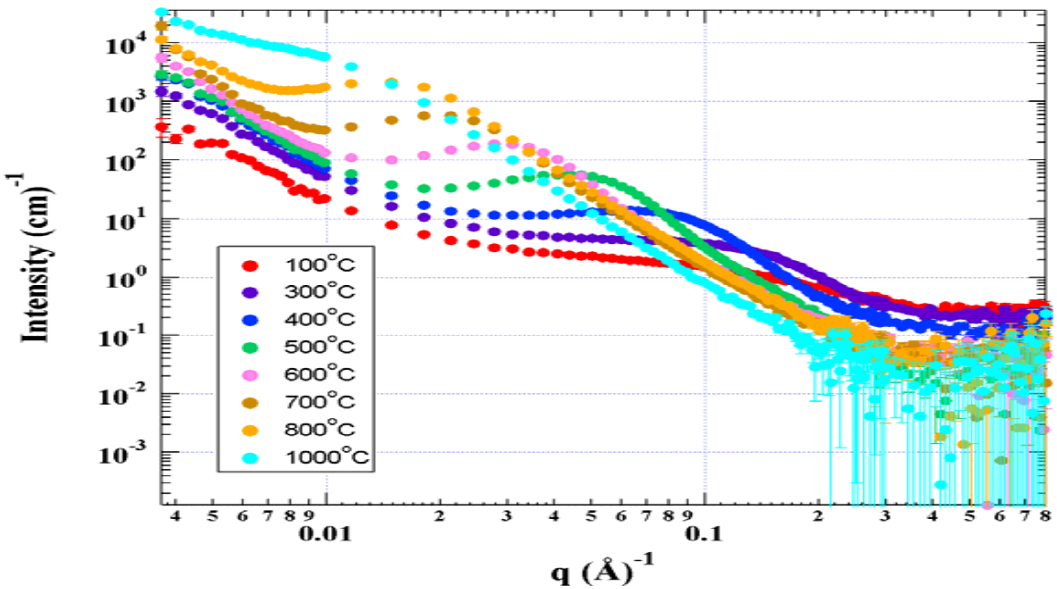

Temperature (°C)	Particle Size (Å)
300	60
400	90
500	134
600	203
700	295
800	423

Effects of heat treatment on zirconia powders produced using the reverse micelle method

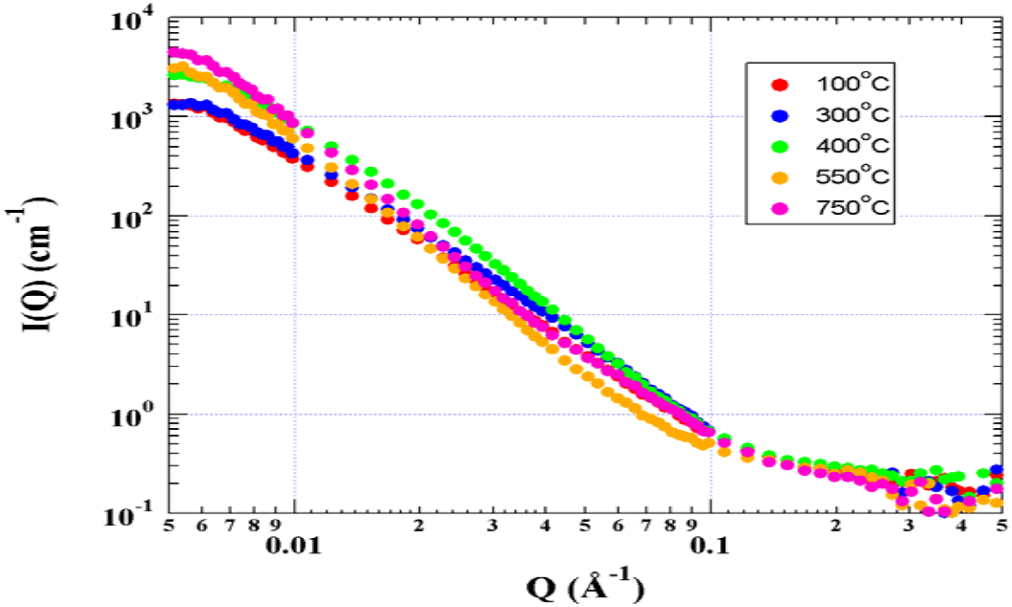

Temperature (°C)	Fractal Dimension	Cutoff Length (Å)
100	2.7	186
200	2.7	197
300	2.7	148
400	2.9	124
550	2.93	223
750	2.9	341

Summary

- **TEM results show the particle size of nanophase zirconia powder is about 10nm and uniform. The shape of nanoparticle is roughly spherical.**
- **The microstructure of the zirconia powder produced using the reverse micelle method is relatively stable under heat treatment below 750°C**
- **Obvious coarsening occurs in the powder produced using the sol-gel method.**

Catalytic Carbons

- **Manufactured from paper-mill sludge**
- **Treated with ZnCl2**
- **Studied using N2 BET and SANS**
- **Contrast-matching experiments with toluene**

Work done at Argonne with N Khalili (IIT) and students, G. Sandi (Chemistry) and Thiyaga (IPNS)

SANS Data

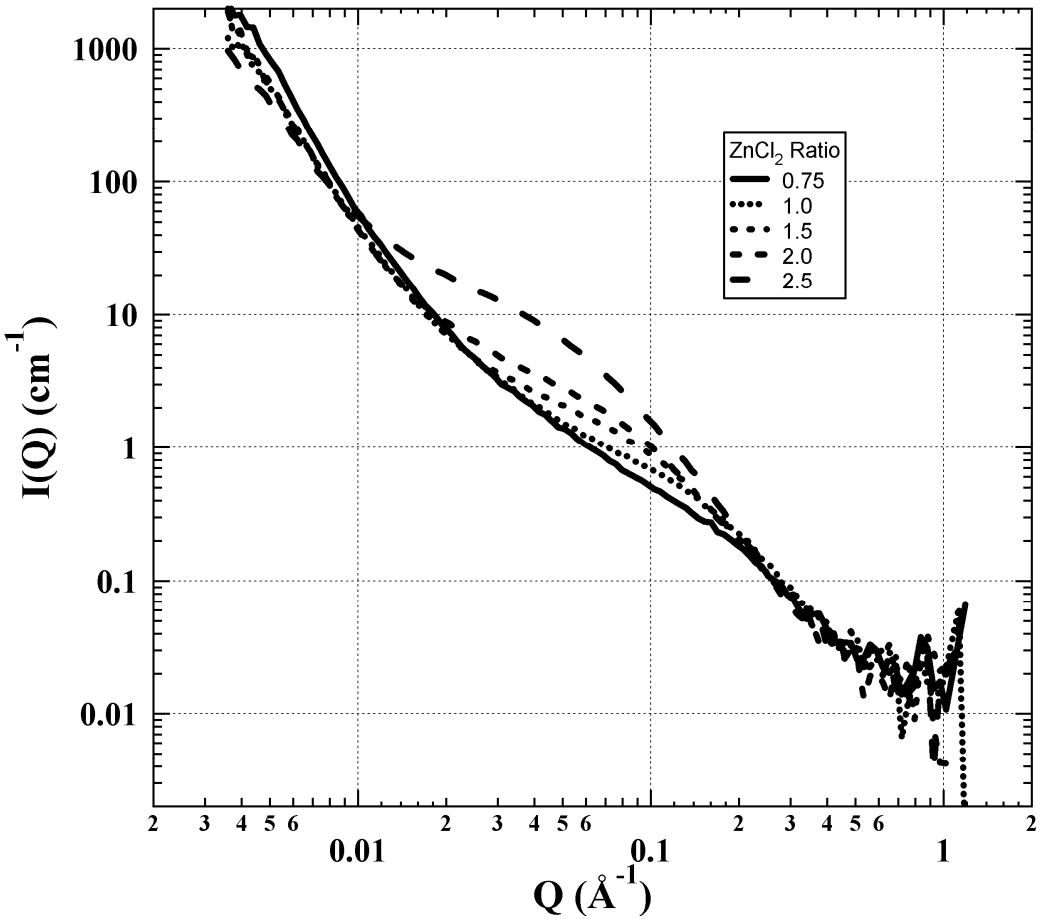
1000
100
10
1
0.1
0.01
I(Q) (cm-1)
2 3 4 5 6
0.01
2 3 4 5 6
0.1
2 3 4 5 6
1
2
Q (Å-1)
ZnCl2 Ratio
0.75
1.0
1.5
2.0
2.5

Sample Unified Fit

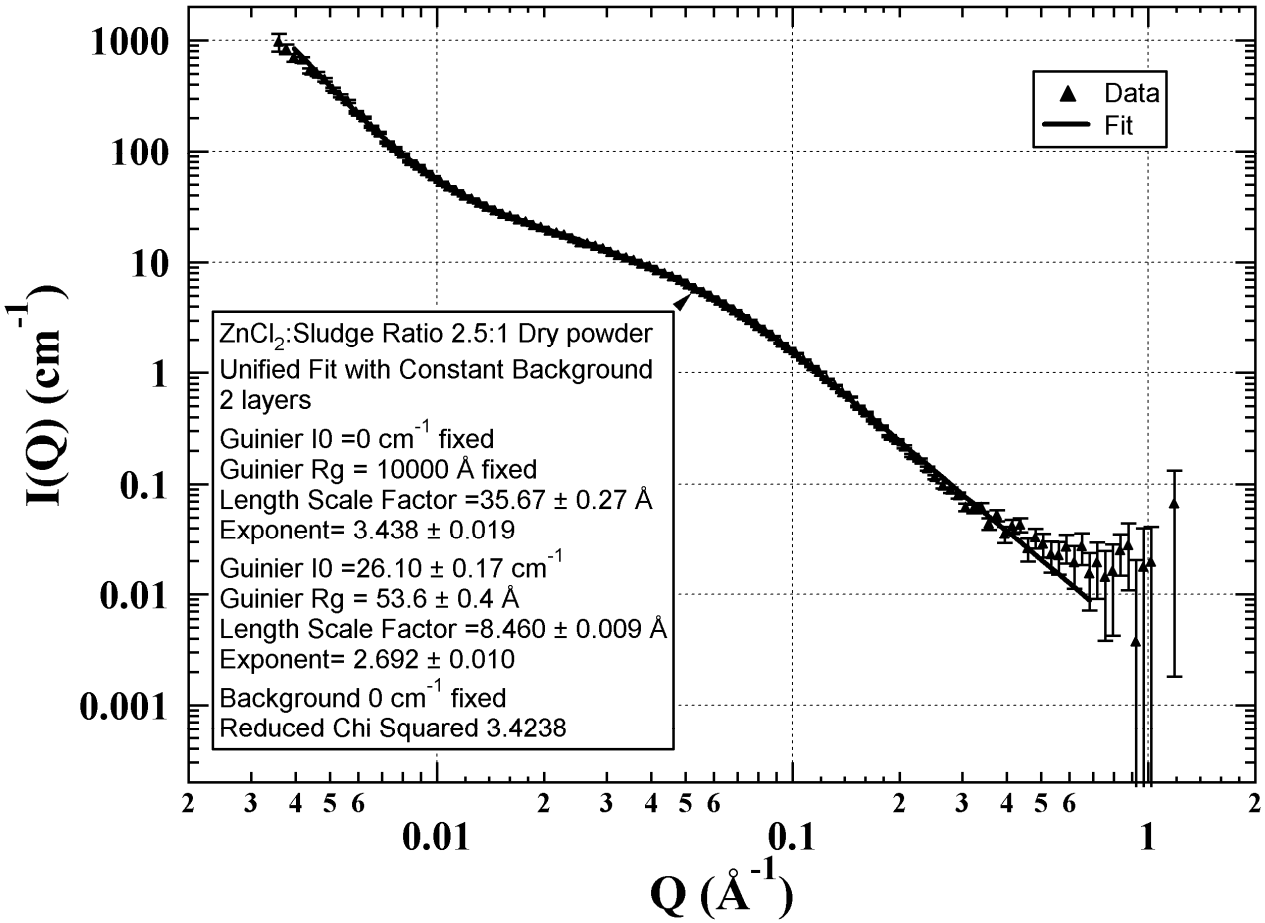

Fit Parameters

$ZnCl_2$:Sludge ratio	Low Q Power Law exponent	Surface Fractal Dimension	High Q Power Law exponent	High Q Radius of Gyration (Å)	High Q Guinier I0 Prefactor (cm^{-1})	High Q Power Law Length Scale (Å)
0.75:1	3.779(23)	2.221(23)	1.528(5)	119.5(25)	29.2(18)	15.744(29)
1:1	3.193(9)	2.807(9)	1.94(3)	30.6(13)	2.63(8)	11.04(15)
1.5:1	3.518(11)	2.482(11)	2.343(26)	33.9(7)	4.16(6)	9.80(6)
2:1	3.624(12)	2.376(12)	2.533(17)	39.9(4)	6.98(5)	9.632(29)
2.5:1	3.438(19)	2.562(19)	2.692(10)	53.6(4)	26.10(16)	8.460(9)

Data After Subtraction

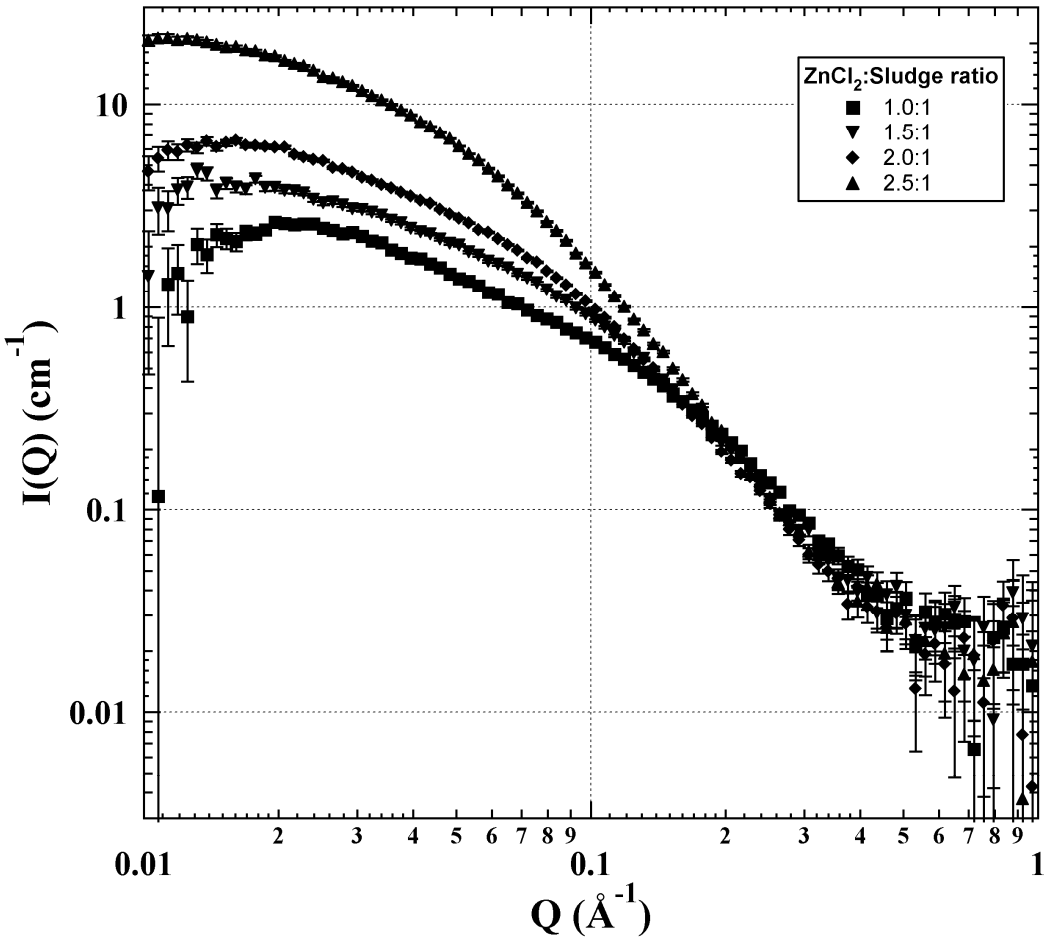

Modified Guinier Analysis

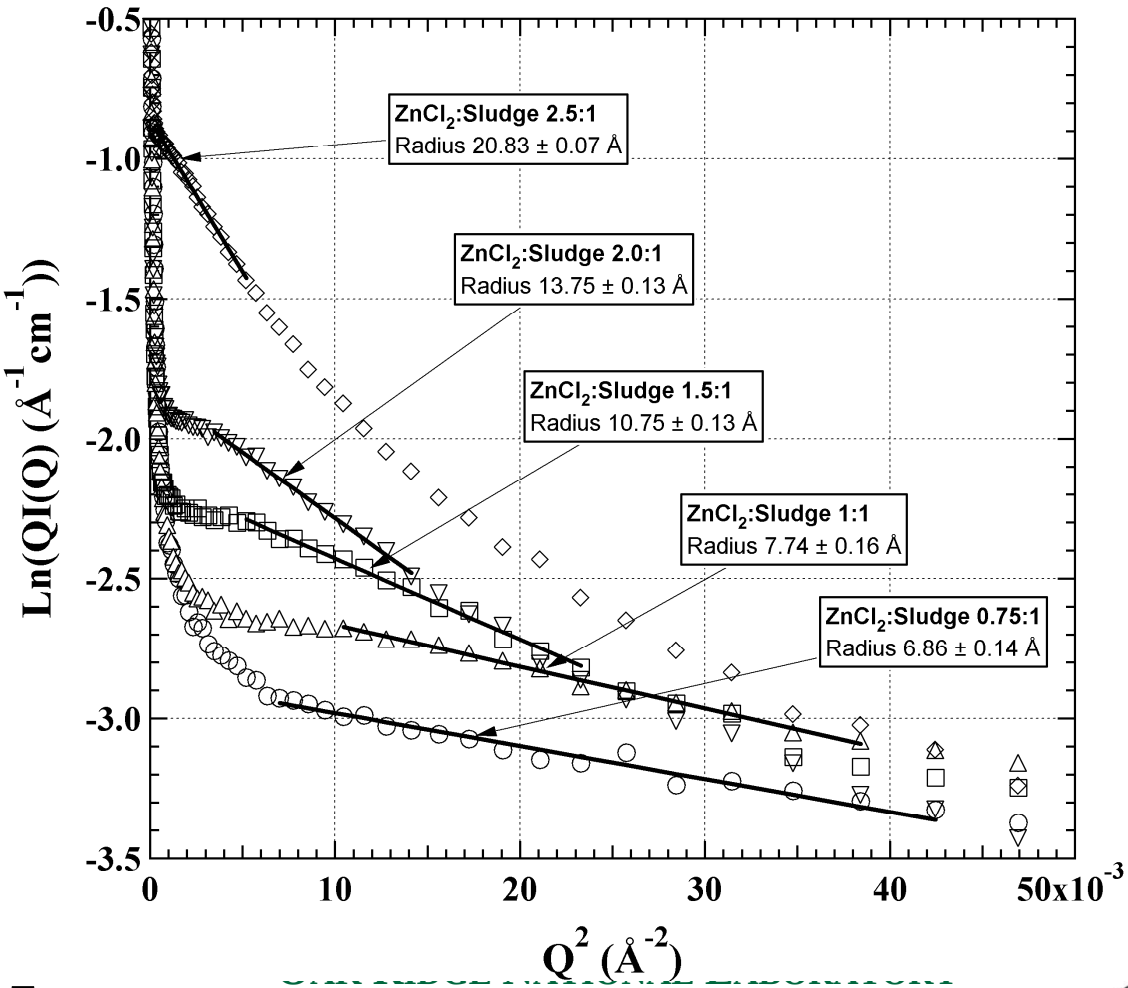

Contrast-Variation Data

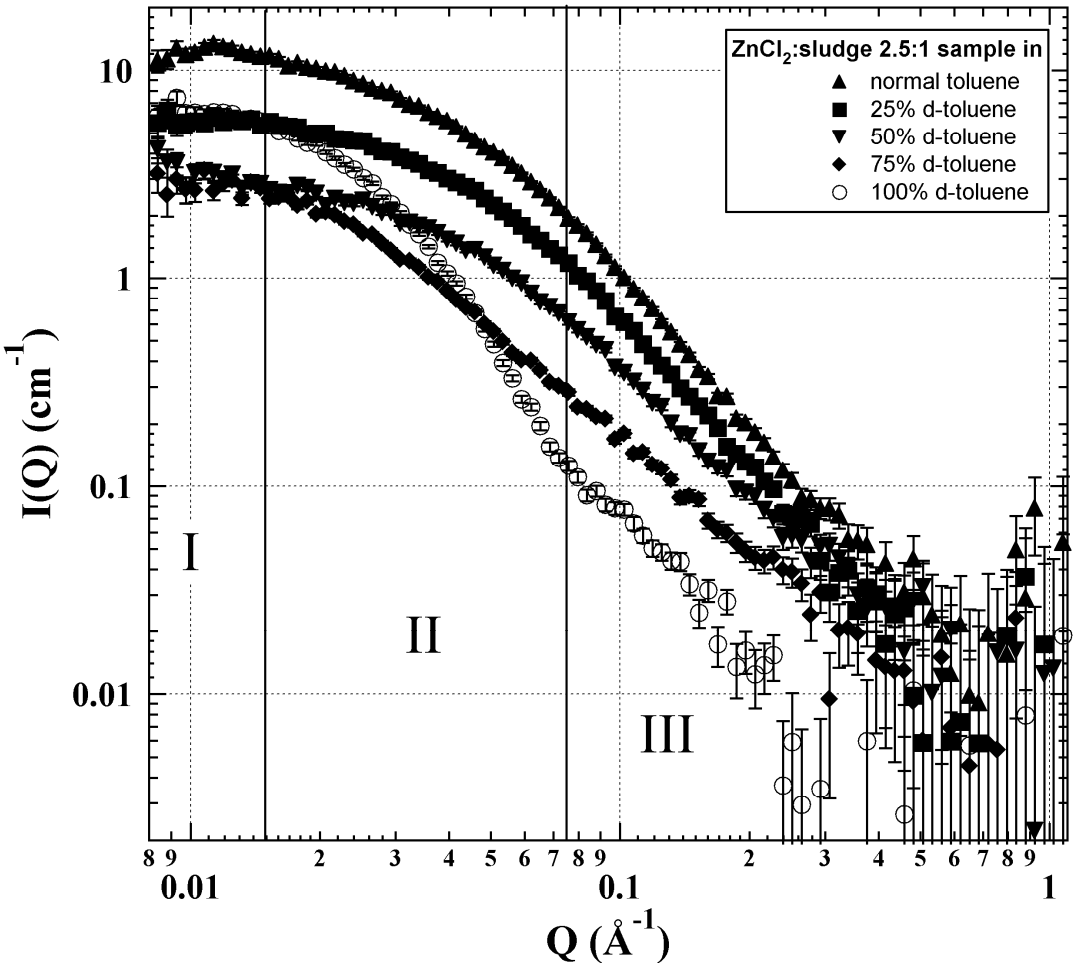

Low-Q Intensity Variation

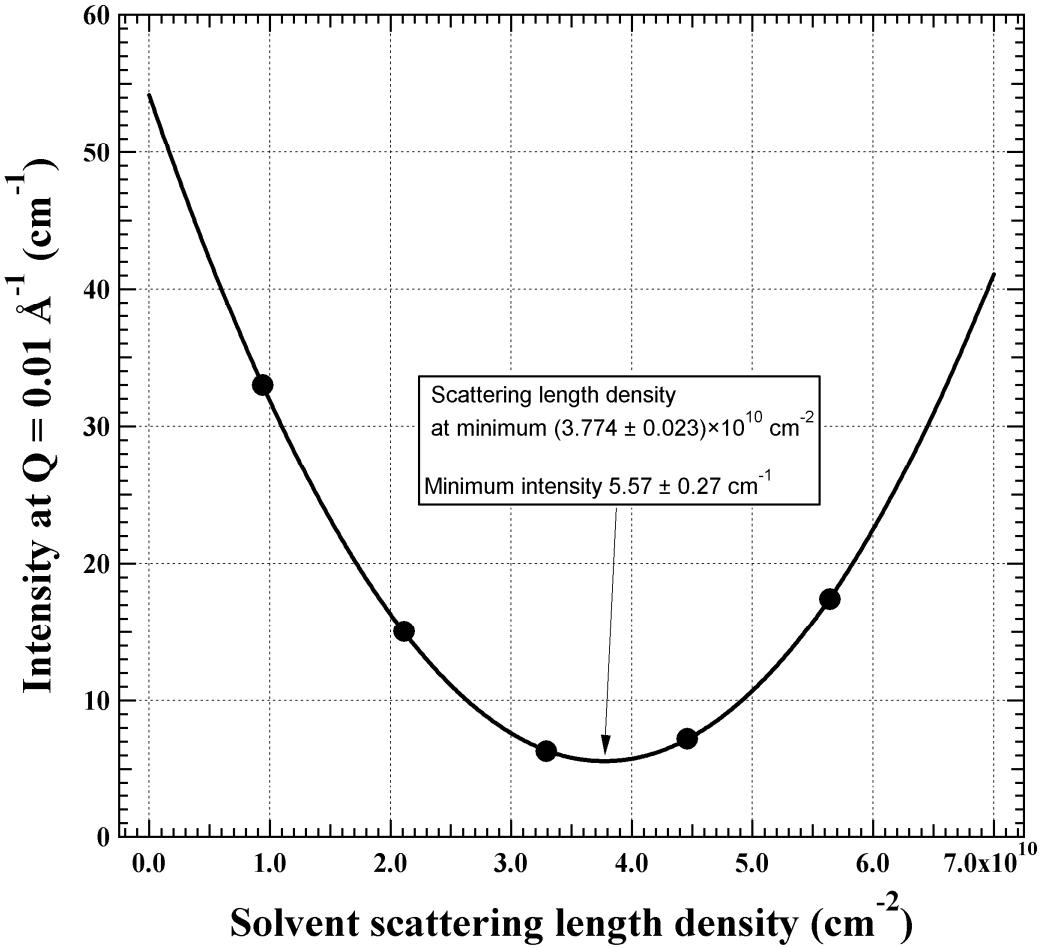

High Q Intensity Variation

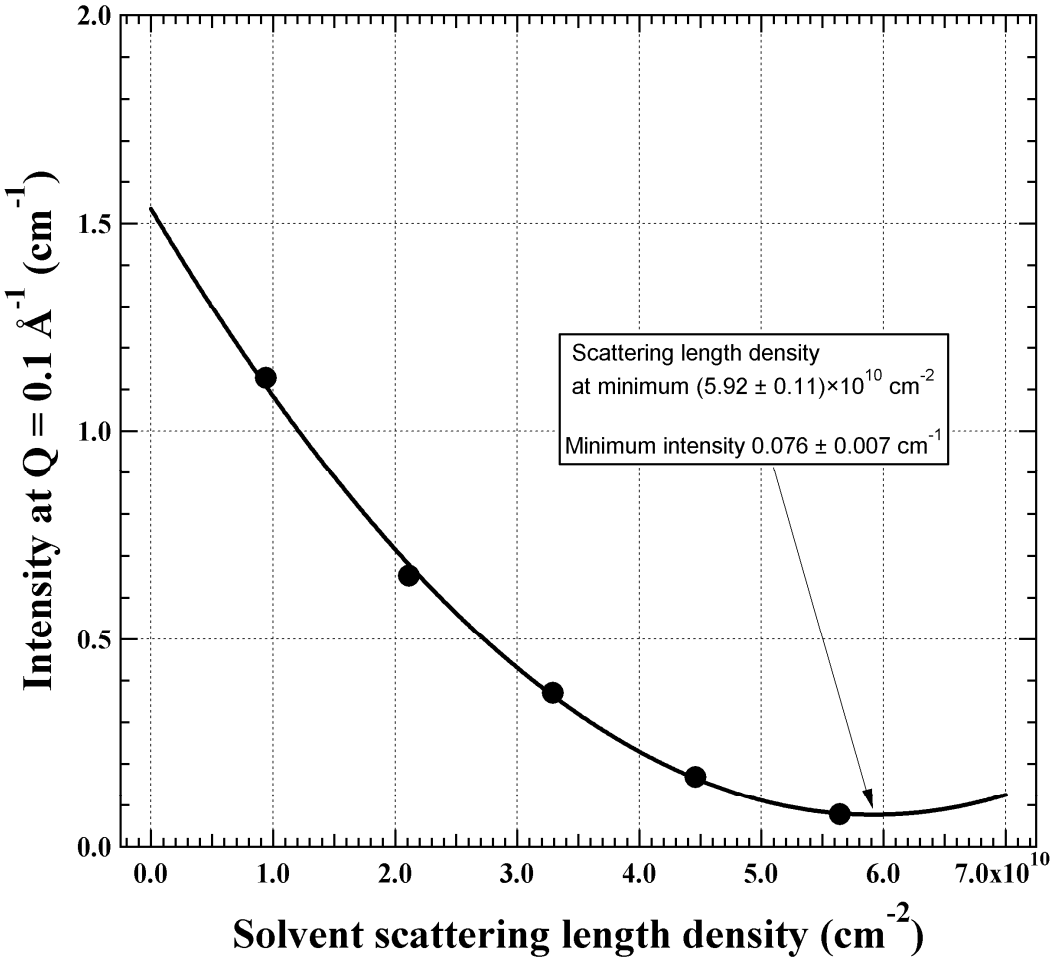

Proposed Model

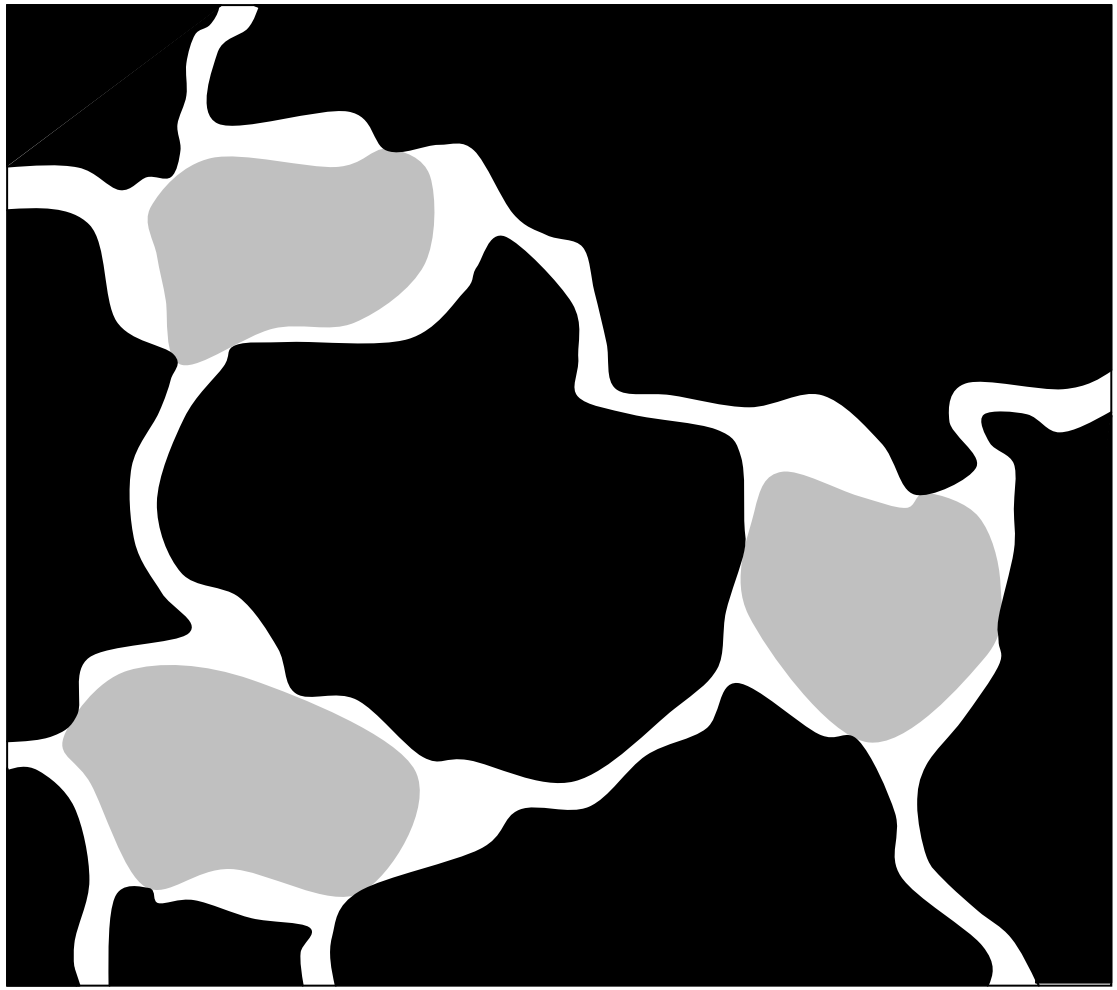

SANS studies of ageing effects and precipitation in germanium- and arsenic sulfide glasses

Eugene Bychkov and Frank Hindle, Universite Littoral, Dunkerque, France

Ken Littrell, IPNS, Argonne National Laboratory

Experiments performed at ILL D22 and LLB PAXY

AsS glasses after 1 year ageing

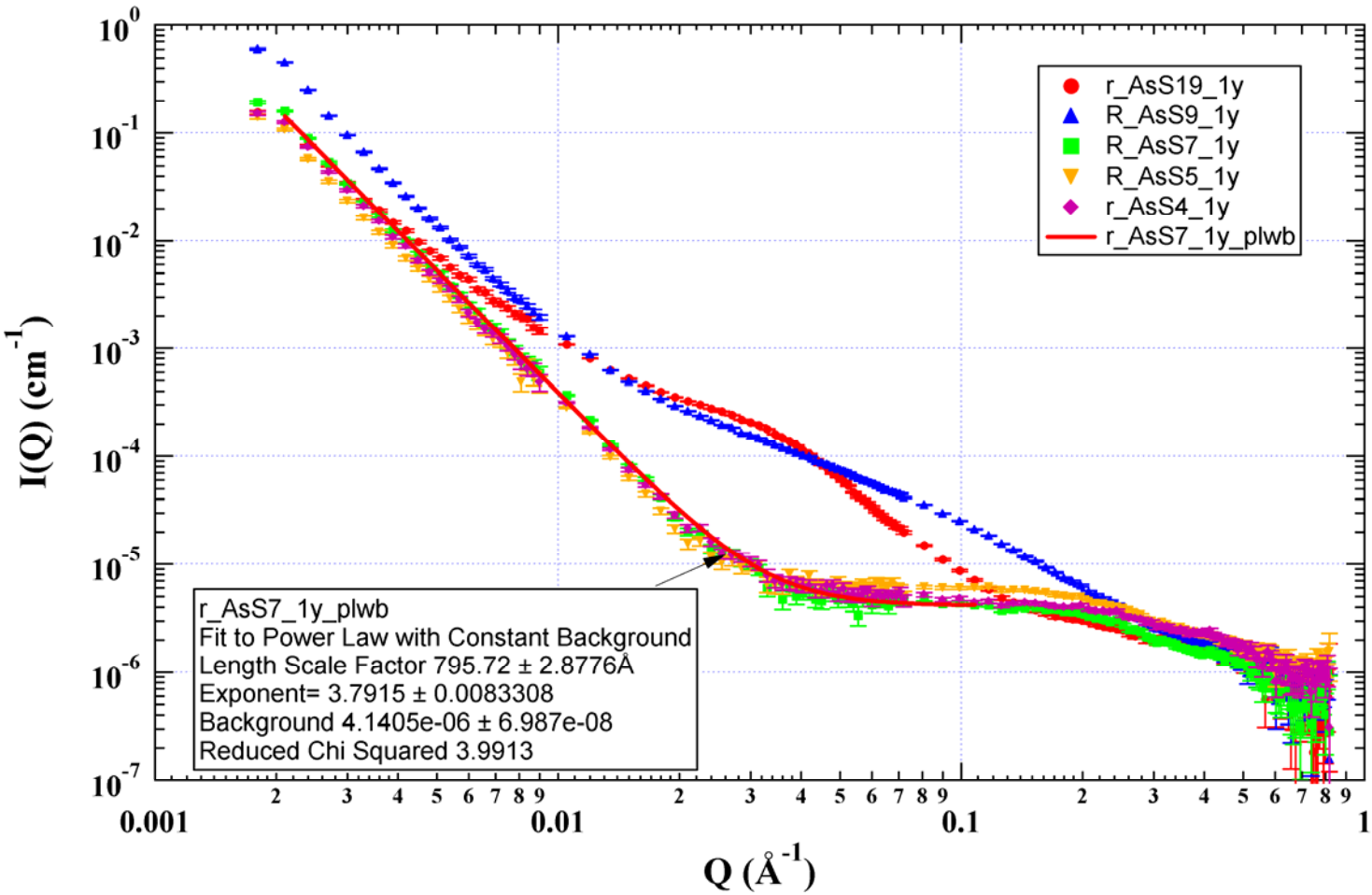

Arsenic sulfide glass conclusions

- **Low sulfur content AsS glasses exhibit only a slight increase in scattering with ageing**
- **The AsS 9 sample showed a dramatic increase in low-q power-law scattering and contained particles at 2 months that grew into long, rodlike structures at a year**
- **At high q, the AsS19 At high q the fresh sample exhibits the presence of compact particles with a Rg of 9 A At one month, the sample shows the presence of particles with a Rg of 49 A ,. Again the intensity increased dramatically over a year**
- **The low q power law was consistent with a surface fractal for all of the samples studied**

Germanium sulfide glass conclusions

- **At low Q the scattering shows a power law of -4 in the two samples with the lowest sulfur concentration, GeS1.29 and GeS2, consistent with scattering from a large-scale smooth surface. . The GeS2.5 and GeS3 samples on the other hand, have low-q scattering with a power law exponent of about -2.7, characteristic of the scattering from a mass fractal. The GeS3.5 data has a low-Q exponent of -4.**
- **In the two most concentrated samples, GeS7 and GeS9, Modified Guinier analysis for rodlike forms shows that these structures are indeed rodlike, with a cross-sectional radius of gyration Rc of 13 Å for the GeS7 sample and 26 Å for the GeS9 sample.**

Geology and/or petrology

- **Samples have much in common with those just mentioned**
- **Mass-or surface fractal behavior over many orders of magnitude**
- **Fractal pore networks characteristic of coals**
- **Fractal structure changes and knees in the curves indicating characteristic lengths reflect the history of heat treatment in marbles**
- **For examples, search SANS+Coal, SANS+ Marble**

Structural and Industrial Alloys: Small-angle neutron scattering analysis of the precipitation behaviour in a maraging steel

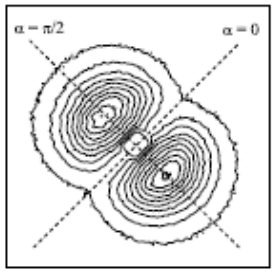

Figure 3

Isointensity lines of a detector image at a distance of 1 m (Sample 3, 12 h/748 K).

$$(\Delta\eta)^2 = (\Delta\eta_{\mathrm{nuc}})^2 + (\Delta\eta_{\mathrm{mag}})^2 \cdot \sin^2\alpha \,. \qquad (5)$$

Thus, the nuclear cross section is measured at $\alpha = 0$, while the sum of nuclear and magnetic cross section is measured at $\alpha = \pi/2$. The magnetic cross section can be calculated by subtracting the masurement at $\alpha = 0$ from the measurement at $\alpha = \pi/2$.

P. Staron,[a]* B. Jamnig,[b] H. Leitner,[c] R. Ebner[b] and H. Clemens[a]

[a]Institute for Materials Research, GKSS Research Center, D-21502 Geesthacht, Germany, [b]Materials Center Leoben (MCL), A-8700 Leoben, Austria, and [c]Department of Physical Metallurgy and Materials Testing, University of Leoben, A-8700 Leoben, Austria. E-mail: Staron@gkss.de

J. Appl. Cryst. (2003). **36**, 415–419

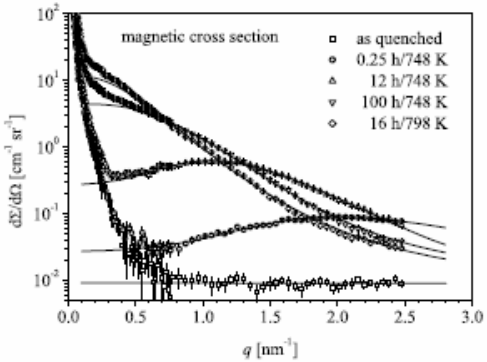

Figure 4

Magnetic SANS cross section. Symbols: measured data; solid lines: calculated curves.

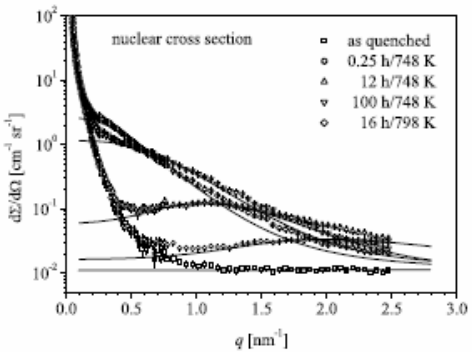

Figure 5

Nuclear SANS cross section. Symbols: measured data; solid lines: calculated curves.

Small-angle neutron scattering investigations of magnetic nanostructures using polarized neutrons: SANSPOL

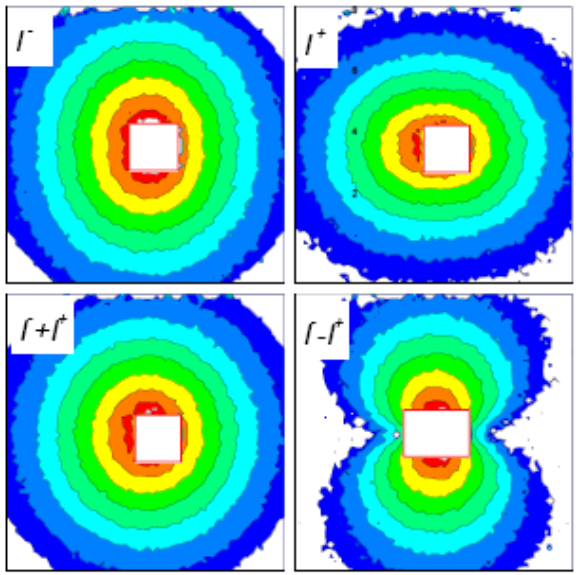

$$I^{-}(Q,\alpha) = \langle |F^{++}|^2 \rangle + \langle |F^{+-}|^2 \rangle = F_N^2 + \{F_M^2 - 2\,P\,F_N F_M\}\,\sin^2\alpha$$
$$I^{+}(Q,\alpha) = \langle |F^{--}|^2 \rangle + \langle |F^{-+}|^2 \rangle = F_N^2 + \{F_M^2 + 2\,P\varepsilon\,F_N F_M\}\,\sin^2\alpha, \quad (1a)$$

$$[I^{-}(Q,\alpha) + I^{+}(Q,\alpha)]/2 = I(Q,\alpha)_{\text{non-polrised}} = F_N^2 + F_M^2\,\sin^2\alpha\,. \quad (1b)$$

The difference between the intensities of the two polarisation states represents a magnetic-nuclear cross term,

$$I^{-}(Q,\alpha) - I^{+}(Q,\alpha) = 2\,P\,(1+\varepsilon)\,F_N F_M \sin^2\alpha = B_{int}(Q)\,\sin^2\alpha. \quad (1c)$$

$$d\sigma(Q,\alpha)/d\Omega = A(Q) + B^{\pm}(Q)\,\sin^2\alpha. \quad (2)$$

$$FR = I(\mathbf{Q}\perp\mathbf{H}) / I^{+}(\mathbf{Q}\perp\mathbf{H}) = (1+2P\varepsilon\gamma + \gamma^2)/(1-2P\gamma+\gamma^2). \quad (3)$$

$$\gamma = B_{int}(Q) / [2A(Q)P(1+\varepsilon)]. \quad (4)$$

Figure 1
SANSPOL patterns in Fe_3O_4 for neutron spins antiparallel (I^-) and parallel (I^+) to the horizontal field. The arithmetic mean $[(I^-) + (I^+)]/2$ corresponds to the 2D pattern of non-polarised neutrons. The difference (I^-)-(I^+) yields the interference term [equation (1c)].

Crystalline and magnetic nanostructures have been studied by means of small angle neutron scattering. Using polarised neutrons, the relative contrasts are strongly modified which allowed magnetisation, density and composition profiles at surfaces and interfaces to be evaluated. In nanocrystalline Fe_3O_4 embedded in a glass ceramics matrix the magnetic order is strongly disturbed at the surface of the particles, leading to a magnetically inactive layer. In partially crystallised metallic Fe-Si-B-(Nb,Cu) alloys the presence of a non-magnetic interface between Fe_3Si nanocrystals and the amorphous matrix has been demonstrated which breaks the direct ferromagnetic exchange interactions. In Co-ferrofluids the superparamagnetic core is encapsulated by a shell of surfactant molecules which was found to be impenetrable for the solvent.

Albrecht Wiedenmann

J. Appl. Cryst. (2000). 33, 428±432

Superconductivity: Vortex lattice reorientation and anisotropy in MgB2

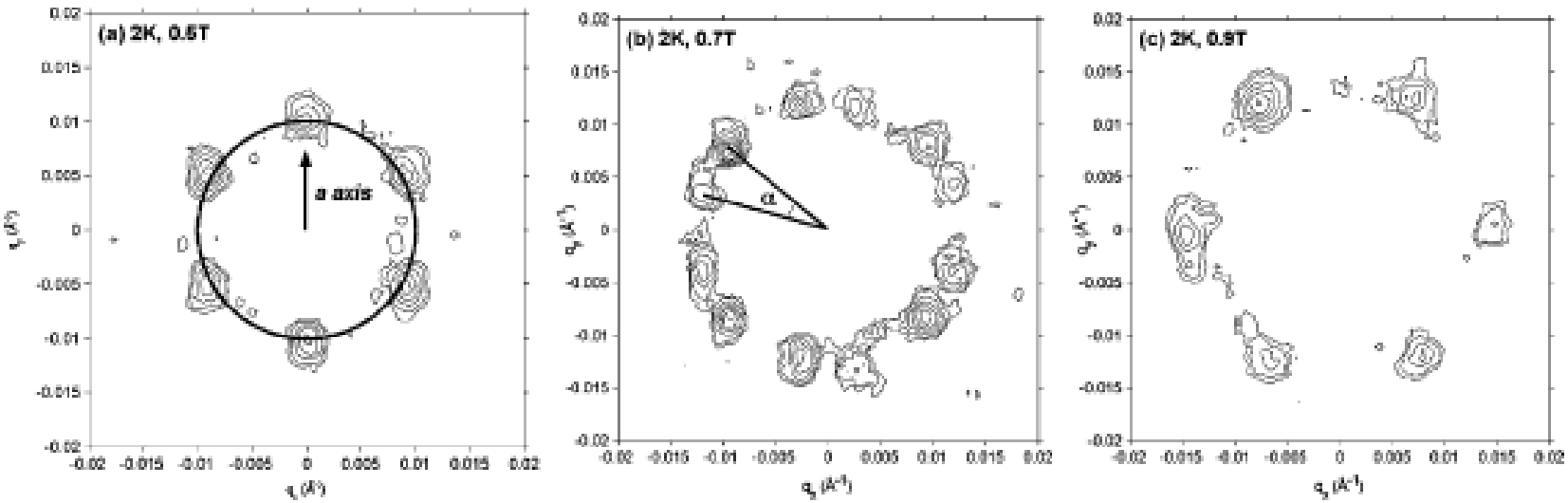

Fig. 1. SANS diffraction patterns from the VL in MgB_2 at 2 K at fields of (a) 0.5 T, (b) 0.7 T and (c) 0.9 T ($B \| c$). The VL splits into two domain orientations of separation angle α, increasing with field until reforming a single rotated domain at high fields (c).